Evanescent Wave Sensors with a Left-Handed Material as a Substrate

Sofyan A. Taya,[1,*] Mazen M. Abadla,[2] Mohamed M. Shabat,[1] and Eman J. El-Farram[1]

[1]*Physics Department, Islamic University, Gaza, P.O. Box 108, Gaza Strip, Palestinian Authority*

[2]*Physics Department, Alaqsa University, Gaza Strip, Palestinian Authority*

(Received April 20, 2011; Revised September 11, 2011)

In this work, we examine analytically the propagation of TE and TM polarized waves in a three-layer slab waveguide with the substrate layer made of a left-handed material of negative and complex permittivity and permeability. The dispersion relation, the penetration depth, and the power flowing through each layer are derived. The effect of the negative optical parameters of the substrate on these parameters is studied in detail. The structure is also treated as an evanescent wave optical sensor. The sensitivity of this sensor is presented and studied with different parameters of the structure.

PACS numbers: 42.82.Et, 81.05.Xj, 78.67.Pt, 07.07.Df

I. INTRODUCTION

Permittivity (ε) and permeability (μ) are the basic physical parameters for describing the medium-electromagnetic wave interaction. They determine the propagating behavior of electromagnetic waves in the medium. For most natural media ε and μ are positive. However, in 1968 Veselago reported the electromagnetics of materials with simultaneously negative ε and μ [1]. These materials are named as left-handed materials (LHMs) (the ordinary ones are called right-handed materials: RHMs), because the wave vector $\mathbf{k}$, the electric field vector $\mathbf{E}$, and the magnetic field vector $\mathbf{H}$ form a left-handed system [1]. Some of the unusual features of waves in LHMs are reversal of the Doppler effect and Cherenkov radiation [1, 2], negative refraction [3], and unusual nonlinearities [4, 5]. LHMs may find a lot of applications in physics and engineering because they have many characteristics different from RHMs. As a result LHMs have received increasing interest from physicists and engineers.

A LHM was constructed by Smith *et al.* [6] using a combination of periodic rods and split rings, and they performed many experiments in the microwave range to point out that the nature of this material is unlike any existing material. The first experimental investigation of a negative index of refraction was achieved by Shelby *et al.* in 2001 [7]. Voskoboynikov *et al.* showed that semiconductor nano-structures built from non-magnetic InAs/GaAs nano-rings can exhibit simultaneously negative effective permittivity and permeability over a certain optical frequency range [8]. The structures are resonant and have this property near the edge of absorption of the nano-rings.

One of the applications of LHM is the so-called superlens, suggested by Pendry [9], in which a parallel slab of the material with $\varepsilon = \mu = -1$ (lossless medium) serves as a focus-free lens. The super lens carries sub-wavelength structural information, which can be reconstructed in the image plane without loss in intensity. That is, the LHM slab can be

used to achieve super-resolution [10]. Theoretical studies on wave-absorption properties of a structure with left- and right-handed materials have been investigated in detail [11, 12]. Recently, left handed materials have been proposed as a mechanism for building cloaking devices [13, 14]. In this mechanism, the object to be cloaked is surrounded by a shell of LHM that affects the passage of light near it. LHMs have been intensely studied in the field of antenna arrays [15, 16]. LHMs showed a remarkable improvement in microwave and millimeter wave antenna arrays. One of the most recent applications of LHMs has been introduced by Taya *et al.* in the field of optical slab waveguide sensors [17]. We showed that using a thin layer of LHM between the guiding layer and the cladding layer can dramatically enhance the sensitivity of slab waveguide sensors.

At present, slab waveguides have been studied intensively as sensor elements for physical, chemical, biological, and medical applications [18–20]. A slab waveguide structure with a step index profile is the most common configuration that is used in the field of optical waveguide sensing. The sensing process is performed by measuring the change of the effective refractive index of a propagating mode when a change of refractive index occurs in the covering medium. If the measurand is homogeneously distributed in the cover, the process is called homogeneous sensing, and it is called surface sensing when the measurand is an ultrathin film at the cladding-guiding layer interface.

In this paper, we present theoretically a three-layer slab waveguide structure in which the substrate is made of isotropic homogeneous lossy material with both ε and μ being simultaneously negative and complex. We study by simulation the effect of the negative parameters of the substrate on the effective refractive index, power, penetration depth, and sensitivity.

II. THEORY

Figure 1 shows the slab waveguide structure under consideration. It consists of a guiding layer of thickness d and optical parameters (ε_f, μ_f), a cladding layer of optical parameters (ε_c, μ_c), and a substrate layer made of a LHM of parameters (ε_s, μ_s). If we consider s-polarized light (TE) and the longitudinal direction to be the z-direction, the electric field can be written as

$$E(x, y, z, t) = [0, E_y(x), 0]e^{i\beta z}e^{-i\omega t}, \tag{1}$$

whereas the magnetic field is given by

$$H(x, y, z, t) = [H_x(x), 0, H_z(x)]e^{i\beta z}e^{-i\omega t}. \tag{2}$$

where β is the z-component of the propagation constant and ω is the angular frequency.

The nonzero components (E_y, H_x, H_z) are related to each other through Maxwell's equations. E_y can be obtained by solving the Helmholtz equation for TE waves in the three layers, which is given by

$$\frac{\partial^2 E_y(x)}{\partial x^2} + k_0^2\left(\varepsilon_i\,\mu_i - N^2\right)E_y(x) = 0, \quad \text{for TE modes,} \tag{3}$$

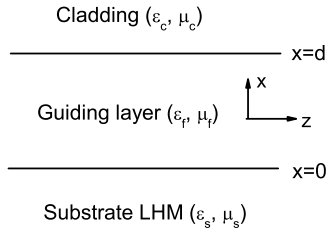

FIG. 1: A schematic diagram of a three-layer slab waveguide with the substrate made of a LHM.

where k_0 is the free space wave number, $i = s$, f, or c indicating the substrate, film or cladding, and N is the effective refractive index of the propagating mode. The solution of Eq. (3) in the three layers is given by

$$E_y = Ae^{-\alpha_c(x-d)}, \quad x > d, \tag{4}$$

$$E_y = B_1 \cos(\alpha_f x) + B_2 \sin(\alpha_f x), \quad 0 < x < d, \tag{5}$$

$$E_y = C\, e^{\alpha_s x}, \quad x < 0, \tag{6}$$

where $\alpha_c = k_0\sqrt{N^2 - \varepsilon_c\mu_c}$, $\alpha_f = k_0\sqrt{\varepsilon_f\mu_f - N^2}$, and $\alpha_s = k_0\sqrt{N^2 - \varepsilon_s\mu_s}$. The constants A, B_1, B_2, and C represent the amplitudes of the wave in the different layers.

The nonzero magnetic field components (H_x and H_z) of the TE modes can be calculated using

$$H_z = \frac{i}{\omega\mu}\frac{\partial E_y}{\partial x} \quad \text{and} \quad H_x = \frac{-k_0 N}{\omega\mu}E_y, \tag{7}$$

where ω is the angular frequency and $\mu = \mu_0\mu_i$ with μ_0 being the free space permeability.

The continuity of the tangential components of the electric and magnetic fields (E_y and H_z) gives rise to the dispersion relation given by

$$\alpha_f d = \tan^{-1}\left(\frac{\alpha_c\ \mu_f}{\alpha_f\ \mu_c}\right) + \tan^{-1}\left(\frac{\alpha_s\ \mu_f}{\alpha_f\ \mu_s}\right) + m\pi, \tag{8}$$

where $m = 0, 1, 2, \ldots$ is the mode order.

We here assume the cladding and guiding layers to be nonmagnetic materials with $\mu_c = \mu_f = 1$, so that dispersion relation can be written as

$$\alpha_f d = \tan^{-1}\left(\frac{\alpha_c}{\alpha_f}\right) + \tan^{-1}\left(\frac{\alpha_s}{\alpha_f\mu_s}\right) + m\pi. \tag{9}$$

In a similar manner, for p-polarized light (TM) the magnetic and electric fields are respectively given by

$$H(x, y, z, t) = [0, H_y(x), 0]e^{i\beta z}e^{-i\omega t}, \tag{10}$$

$$E(x,y,z,t) = [E_x(x), 0, E_z(x)]e^{i\beta z}e^{-i\omega t}. \tag{11}$$

H_y satisfies the Helmholtz equation which for TM modes takes the form:

$$\frac{\partial^2 H_y(x)}{\partial x^2} + k_0^2\left(\varepsilon_i\mu_i - N^2\right)H_y(x) = 0, \quad \text{for TM modes.} \tag{12}$$

The solution of this equation is given by

$$H_y = ae^{-\alpha_c(x-d)}, \quad x > d, \tag{13}$$

$$H_y = b_1\cos(\alpha_f x) + b_2\sin(\alpha_f x), \quad 0 < x < d, \tag{14}$$

$$H_y = ce^{\alpha_s x}, \quad x < 0. \tag{15}$$

The nonzero electric field components (E_x and E_z) of the TM modes can be calculated using

$$E_z = \frac{-i}{\omega\varepsilon}\frac{\partial H_y}{\partial x} \quad \text{and} \quad E_x = \frac{k_0 N}{\omega\varepsilon}H_y, \tag{16}$$

where $\varepsilon = \varepsilon_i\varepsilon_0$ with ε_0 being the free space permittivity. The continuity of the tangential components gives

$$\alpha_f d = \tan^{-1}\left(\frac{\alpha_c\varepsilon_f}{\alpha_f\varepsilon_c}\right) + \tan^{-1}\left(\frac{\alpha_s\varepsilon_f}{\alpha_f\varepsilon_s}\right) + m\pi. \tag{17}$$

When light waves are coupled into a slab waveguide, they are guided through the wave-guiding film by a series of total internal reflections at the cladding-film and substrate-film interfaces. A standing wave, also known as an evanescent wave, is formed at each point of total internal reflection along the propagation direction. The evanescent wave penetrates the surrounding media to some extent, called the penetration depth, which is given by

$$\Delta x_i = \frac{1}{2k_0 N}\frac{\partial\phi_i}{\partial\gamma} \tag{18}$$

where γ is the incidence angle of the beam,

$$\phi_c = 2\tan^{-1}\left(\frac{\alpha_c}{\alpha_f}\right) \quad \text{and} \quad \phi_s = 2\tan^{-1}\left(\frac{\alpha_s}{\alpha_f\mu_s}\right) \quad \text{for TE modes,} \tag{19}$$

$$\phi_c = 2\tan^{-1}\left(\frac{\alpha_c\varepsilon_f}{\alpha_f\varepsilon_c}\right) \quad \text{and} \quad \phi_s = 2\tan^{-1}\left(\frac{\alpha_s\varepsilon_f}{\alpha_f\varepsilon_s}\right) \quad \text{for TM modes.} \tag{20}$$

Making use of the relation $N = \sqrt{\varepsilon_f\mu_f}\sin(\gamma)$ to differentiate Eqs. (19) and (20), we obtain

$$\Delta x_c = \frac{1}{\alpha_c} \quad \text{for TE modes,} \tag{21}$$

$$\Delta x_s = \frac{\mu_s}{\alpha_s}\frac{(\alpha_f^2+\alpha_s^2)}{(\alpha_f^2\mu_s^2+\alpha_s^2)} \quad \text{for TE modes,} \tag{22}$$

$$\Delta x_c = \frac{\varepsilon_c(\alpha_f^2+\alpha_c^2)}{\alpha_c\varepsilon_f(\alpha_f^2[\varepsilon_c/\varepsilon_f]^2+\alpha_c^2)} \quad \text{for TM modes,} \tag{23}$$

$$\Delta x_s = \frac{\varepsilon_s(\alpha_f^2+\alpha_s^2)}{\alpha_s\varepsilon_f(\alpha_f^2[\varepsilon_s/\varepsilon_f]^2+\alpha_s^2)} \quad \text{for TM modes.} \tag{24}$$

When the refractive index of an analyte uniformly distributed in the cladding changes, variations in the effective refractive index (N) occur. In this case, the sensitivity of the slab waveguide sensor is defined as the rate of change of the effective refractive index under an index change of the cladding. Differentiating Eqs. (9) and (17) with respect to N, we obtain

$$S = \frac{\partial N}{\partial n_c} = \frac{n_c\,\alpha_f^2}{\alpha_c\,N\,(\alpha_f^2+\alpha_c^2)}\left[d+\frac{1}{\alpha_c}+\frac{\mu_s(\alpha_f^2+\alpha_s^2)}{\alpha_s(\alpha_f^2\mu_s^2+\alpha_s^2)}\right]^{-1} \quad \text{for TE modes,} \tag{25}$$

$$S = \frac{\partial N}{\partial n_c} = \frac{n_f^2\,\alpha_f^2\,n_c\,\eta_1}{k_0^2\,N\,\alpha_c}\left[\frac{n_f^2\,n_c^2\,\eta_2}{\alpha_c}+\frac{\varepsilon_s\,\varepsilon_f\,\eta_3}{\alpha_s}+d\right]^{-1} \quad \text{for TM modes,} \tag{26}$$

where $\eta_1 = \frac{k_0^2\ n_c^2+2\alpha_c^2}{\alpha_f^2 n_c^4+\alpha_c^2 n_f^4}$, $\eta_2 = \frac{\alpha_f^2+\alpha_c^2}{\alpha_f^2 n_c^4+\alpha_c^2 n_f^4}$, and $\eta_3 = \frac{\alpha_f^2+\alpha_s^2}{\alpha_f^2\varepsilon_s^2+\alpha_s^2\varepsilon_f^2}$.

It is of high importance to study the effect of the negative parameters on the power associated with the propagating mode in each layer. The energy flux per unit length is given by

$$P_{\text{total}} = \frac{k_0 N}{2\,\omega}\int_{-\infty}^{\infty}\frac{|E_y(x)|^2}{\mu(x)}\,dx \quad \text{for TE modes,} \tag{27}$$

$$P_{\text{total}} = \frac{k_0 N}{2\,\omega}\int_{-\infty}^{\infty}\frac{|H_y(x)|^2}{\varepsilon(x)}dx \quad \text{for TM modes.} \tag{28}$$

Using Eqs. (4–6), the power flowing in each layer for TE modes is

$$P_c = \frac{\sigma_1\,\alpha_f^2}{2\,\alpha_c^3}\left[\sin(\alpha_f d)-\frac{\alpha_s}{\alpha_f\mu_s}\cos(\alpha_f d)\right]^2, \tag{29}$$

$$P_f = \sigma_1\left[\frac{1}{2}(d+\sigma_2)+\frac{\alpha_s^2}{2\alpha_f^2\mu_s^2}(d-\sigma_2)+\frac{\alpha_s}{\alpha_f^2\mu_s}\sin^2(\alpha_f d)\right], \tag{30}$$

$$P_s = \frac{\sigma_1}{2\mu_s\ \alpha_s}, \tag{31}$$

where

$$\sigma_1 = \frac{N\ k_0\ |C|^2}{2\omega\ \mu_0}, \tag{32}$$

$$\sigma_2 = \frac{\sin\left(2\alpha_f d\right)}{2\alpha_f}. \tag{33}$$

In a similar manner, if we substitute for $H_y(x)$ from Eqs. (13–15) into Eq. (28), we get

$$P_c = \frac{\sigma_3\,\alpha_f^2\,\varepsilon_c^2}{2\varepsilon_c\ \alpha_c^3\ \varepsilon_f^2}\left[\sin(\alpha_f d) - \frac{\alpha_s\ \varepsilon_f \cos(\alpha_f d)}{\alpha_f \varepsilon_s}\right]^2, \tag{34}$$

$$P_f = \frac{\sigma_3}{\varepsilon_f}\left[\frac{1}{2}(d+\sigma_2\,) + \frac{\alpha_s^2\varepsilon_f^2}{2\alpha_f^2\varepsilon_s^2}(d-\sigma_2) + \frac{\alpha_s\varepsilon_f}{\alpha_f^2\varepsilon_s}\sin^2(\alpha_f d)\right], \tag{35}$$

$$P_s = \frac{\sigma_3}{2\varepsilon_c\alpha_s}, \tag{36}$$

where

$$\sigma_3 = \frac{N\,k_0\ |C|^2}{2\omega\varepsilon_0}. \tag{37}$$

III. RESULTS AND DISCUSSION

In our calculations below, we consider the analyte to be water of refractive index 1.3304, the guiding layer to have a refractive index $n_f = 1.75$ at a wavelength $\lambda = 632.8$ nm, and the substrate to be a LHM with negative ε and μ. Lossless LHM only represents an ideal case, which cannot be realized in the present designs. However, LHMs with a minimal absorption coefficient were recently proposed [21]. LHMs with minimal absorption coefficients have shown interesting features. It was verified that LHMs with low loss can focus light onto an area smaller than a square wavelength in near fields [22, 23]. This super-resolution is attributed to an important feature of LHMs, which is amplification of evanescent waves [10]. For these reasons, in the present work we treat LHMs with ε and μ having the form $\varepsilon_s = \varepsilon_r + 0.001i$ and $\mu_s = \mu_r + 0.001i$ with ε_r and μ_r both negative. Based on these assumptions, we solve numerically the dispersion relations given by Eqs. (9) and (17) for the effective index N. To investigate the behavior of the effective refractive index, power, penetration depth, and the sensitivity of the waveguide under consideration,

the thickness of the guiding is changed from 300 nm to 1500 and all these parameters were calculated and plotted with the thickness of the guiding layer for different ε_r and μ_r.

In some of the following figures, insets are plotted for better view whenever the curves are close to each other.

Figures 2 and 3 show the real part of the effective index versus the thickness of the guiding layer for different values of the real part of the substrate permittivity for TE and TM modes. Similarly, Figs. 4 and 5 show the same for different values of the real part of the substrate permeability. Increasing of the effective refractive index towards the value of the guiding layer refractive index is a well known behavior. The new features that can be extracted from the figures is that for a given guiding layer thickness, $\mathrm{Re}(N)$ of the TE modes is enhanced when the absolute value of the real part of ε_s increases (Fig. 2), and the situation is reversed when the absolute value of the real part of μ_s increases (Fig. 4). The behavior of the $\mathrm{Re}(N)$ of TM modes is completely opposite to that of TE modes, as seen in Figs. 3 and 5. We also compare the case of a LHM substrate with the conventional case in which the substrate is made of a RHM (glass) with $\varepsilon_s = 2.25$ (corresponding to a refractive index of 1.5) and $\mu_s = 1$. It is clear that the effective index of the RHM substrate is less than that of a LHM substrate. This behavior of the effective refractive index can be attributed to the following argument. The effective refractive index of a propagating mode is determined by the thickness of the guiding layer and constitutive parameters of the materials constituting the waveguide. For a constant guiding layer thickness it is dependent solely on the dielectric permittivity and magnetic permeability of the media constituting the waveguide. In Figs. 2–5, we have assumed a RHM substrate with $\varepsilon_s = 2.25$ and $\mu_s = 1$ and a LHM substrate with $|\mathrm{Re}(\varepsilon_s)|$ ranging between 4–8 and $|\mathrm{Re}(\mu_s)|$ ranging between 3 and 7. Therefore, the enhancement in the effective refractive index in case of the LHM substrate over the case of the RHM substrate is obviously justified. It is simply due to the high values assumed for $|\mathrm{Re}(\varepsilon_s)|$ and $|\mathrm{Re}(\mu_s)|$.

Moreover, when the substrate is a LHM, we have observed a little enhancement in the effective refractive index when $|\mathrm{Re}(\varepsilon_s)|$ increases for TE modes (Fig. 2) and when $|\mathrm{Re}(\mu_s)|$ increases for TM modes (Fig. 5). This is attributed to the same reason mentioned above, which is the direct proportionality of N with these parameters. On the other hand, the barely detected decrease in N when $|\mathrm{Re}(\varepsilon_s)|$ increases for TM modes (Fig. 3) and when $|\mathrm{Re}(\mu_s)|$ increases for TE modes (Fig. 4) may be attributed to the second term of the right-hand side of the dispersion relations given by Eqs. (9) and (17). In these terms, we have $1/\mu_s$ for TE modes and $1/\varepsilon_s$ for TM modes.

The real part of the power flowing in the guiding layer as a function of the guiding layer thickness for different values of the real part of the substrate permittivity is shown in Figs. 6 and 7 for TE and TM modes, respectively. The dependence of the real part of the power flowing in the guiding layer on the guiding layer thickness for different values of the real part of the substrate permeability is depicted in Figs. 8 and 9 for TE and TM modes. In all the Figures (6–9), the case of RHM substrate (glass) with $\varepsilon_s = 2.25$ (corresponding to a refractive index of 1.5) and $\mu_s = 1$ has the minimum power in the guiding layer region. This doesn't mean the guiding layer power can always be enhanced by using a substrate of a LHM with any values of ε_s and μ_s. This enhancement is dependent on the chosen

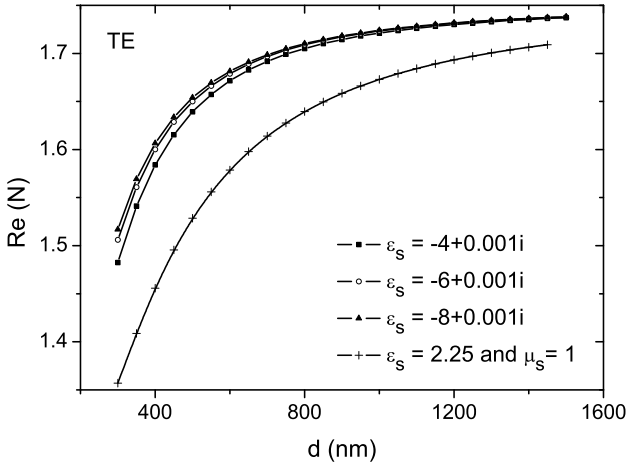

FIG. 2: The real part of the effective refractive index of the propagating mode versus the thickness of the guiding layer for different values of the substrate permittivity for $\lambda = 632.8$ nm, $n_c = 1.33$, $n_f = 1.75$, and $\mu_s = -1 + 0.001\text{i}$ (TE mode).

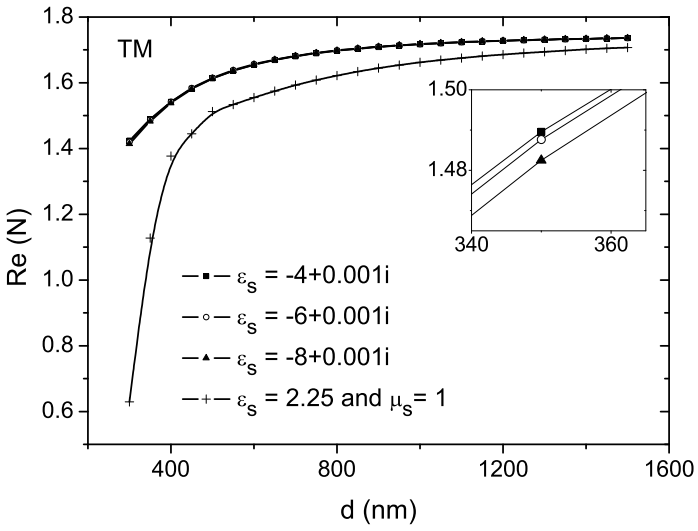

FIG. 3: The real part of the effective refractive index of the propagating mode versus the thickness of the guiding layer for different values of the substrate permittivity for $\lambda = 632.8$ nm, $n_c = 1.33$, $n_f = 1.75$, and $\mu_s = -1 + 0.001\text{i}$ (TM mode).

parameters of the structure. For example, in Figs. 6 and 7, if we consider $|\varepsilon_s| < 4$, this enhancement undergoes a substantial reduction until the power in the guiding layer has values less than that of the case of $\varepsilon_s = 2.25$ and $\mu_s = 1$. Taking $|\mu_s| > 7$ in Fig. 8 or $|\mu_s| < 2$ in Fig. 9 leads to less enhancement in the guiding layer power.

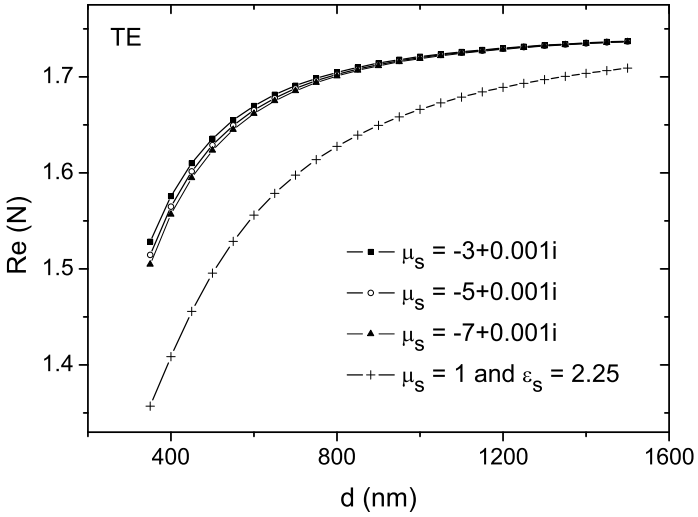

FIG. 4: The real part of the effective refractive index of the propagating mode versus the thickness of the guiding layer for different values of the substrate permeability for $\lambda = 632.8$ nm, $n_c = 1.33$, $n_f = 1.75$, and $\varepsilon_s = -4 + 0.001\mathrm{i}$ (TE mode).

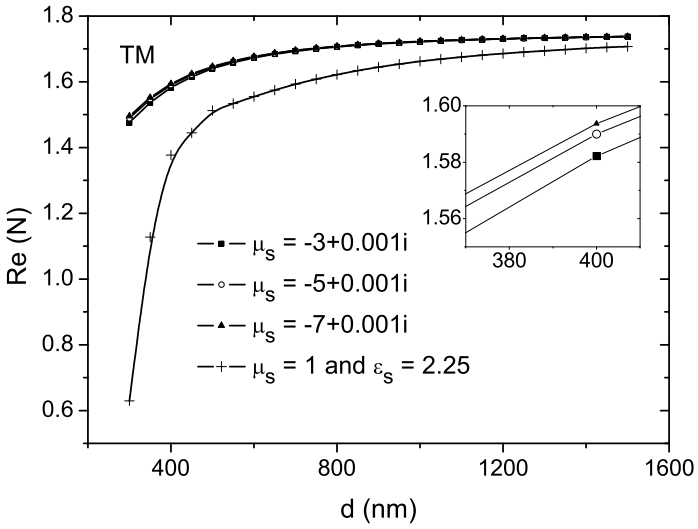

FIG. 5: The real part of the effective refractive index of the propagating mode versus the thickness of the guiding layer for different values of the substrate permeability for $\lambda = 632.8$ nm, $n_c = 1.33$, $n_f = 1.75$, and $\varepsilon_s = -4 + 0.001\mathrm{i}$ (TM mode).

Figures 10–13 show the dependence of the real part of the power flowing in the substrate layer upon the thickness of the guiding layer. They also show this dependence for

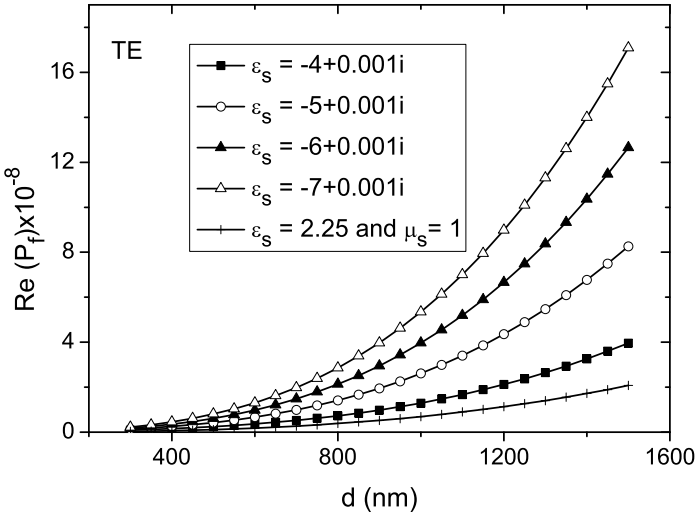

FIG. 6: The real part of the power flowing in the guiding layer versus the thickness of the guiding layer for different values of the substrate permittivity for $\lambda = 632.8$ nm, $n_c = 1.33$, $n_f = 1.75$, and $\mu_s = -1 + 0.001\text{i}$ (TE mode).

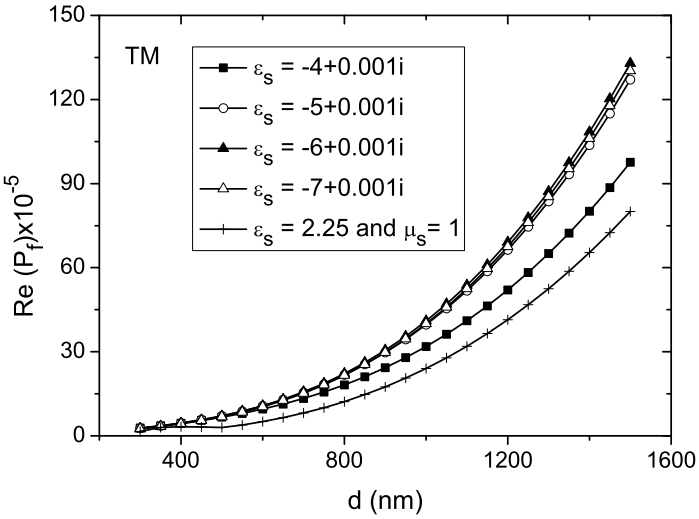

FIG. 7: The real part of the power flowing in the guiding layer versus the thickness of the guiding layer for different values of the substrate permittivity for $\lambda = 632.8$ nm, $n_c = 1.33$, $n_f = 1.75$, and $\mu_s = -1 + 0.001\text{i}$ (TM mode).

different values ε_s and μ_s. The negative value of the substrate power is the most important feature that can be seen in these figures. This is one of the main differences between left-handed and right-handed materials. In a RHM, the Poynting vector $\boldsymbol{S}$ always forms a

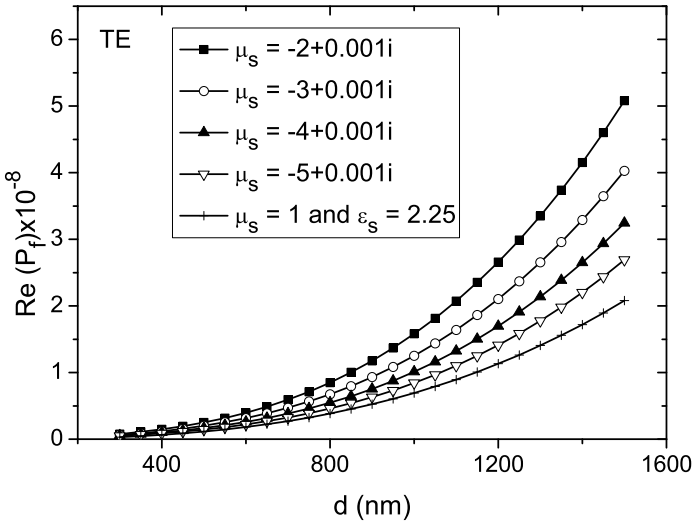

FIG. 8: The real part of the power flowing in the guiding layer versus the thickness of the guiding layer for different values of the substrate permeability for $\lambda = 632.8$ nm, $n_c = 1.33$, $n_f = 1.75$, and $\varepsilon_s = -4 + 0.001\text{i}$ (TE mode).

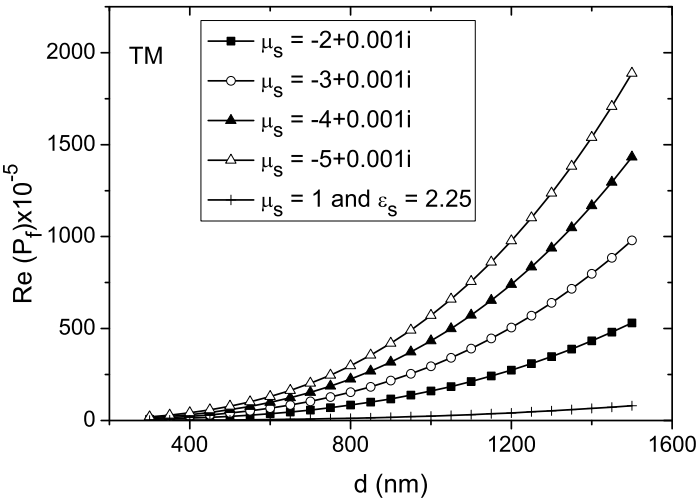

FIG. 9: The real part of the power flowing in the guiding layer versus the thickness of the guiding layer for different values of the substrate permeability for $\lambda = 632.8$ nm, $n_c = 1.33$, $n_f = 1.75$, and $\varepsilon_s = -4 + 0.001\text{i}$ (TM mode).

right-handed set with the vectors $\boldsymbol{E}$ and $\boldsymbol{H}$. Accordingly, for RHMs $\boldsymbol{S}$ and the propagation vector $\boldsymbol{k}$ are in the same direction. However, this is not the case of LHMs in which $\boldsymbol{S}$ and $\boldsymbol{k}$ are in opposite directions. It is well known that the phase velocity and the propagation

vector $\boldsymbol{k}$ are in the same direction for normal materials. Thus, it is clear that LHMs are substances with a so-called negative group velocity, which occurs in particular in anisotropic substances or when there is spatial dispersion [1]. In brief, Figs. 10–13 emphasize the fact that in LHMs the phase velocity is opposite to the energy flow.

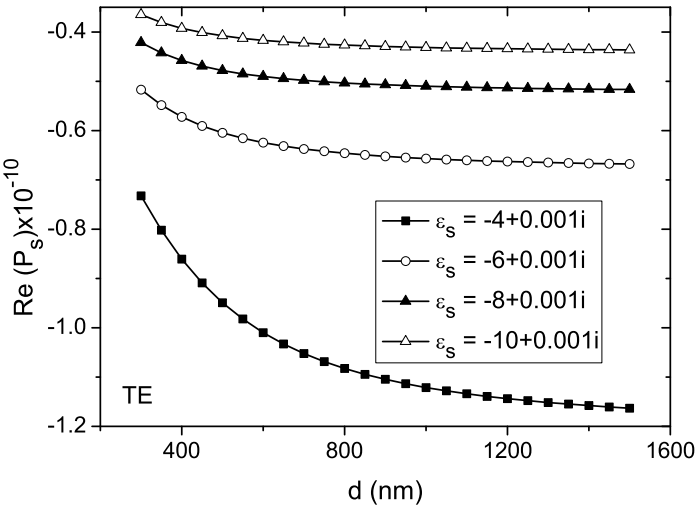

FIG. 10: The real part of the power flowing in the substrate layer versus the thickness of the guiding layer for different values of the substrate permittivity for $\lambda = 632.8$ nm, $n_c = 1.33$, $n_f = 1.75$, and $\mu_s = -1 + 0.001\text{i}$ (TE mode).

The part of the total power flowing in the cladding layer is a significant parameter in the field of slab waveguide optical sensing. The enhancement of this part enhances the sensitivity of the effective refractive index to changes in the refractive index of the cladding. The real part of the power flowing in the cladding layer as a function of the thickness of the guiding layer for different values of the real part of the substrate permittivity is shown in Figs. 14 and 15 for TE and TM modes, respectively. The dependence of the real part of the power flowing in the cladding layer on the guiding layer thickness for different values of the real part of the substrate permeability is depicted in Figs. 16 and 17 for TE and TM modes. In all the Figures (14–17), the case of a RHM substrate (glass) with $\varepsilon_s = 2.25$ (corresponding to a refractive index of 1.5) and $\mu_s = 1$ is shown. In this case (RHM substrate), all figures show the same behavior for $\mathrm{Re}(P_c)$: it approaches zero near cut-off thickness, peaks at a specific value of the guiding layer thickness, and then approaches zero again at high values of the thickness. It is well known that the refractive indices of the layers constituting the waveguide always satisfy the relation $n_c < n_s < n_f$ in a conventional slab waveguide structure with RHMs. The effective refractive index of such a structure is usually greater than n_s and less than n_f. At a certain thickness, called the cut-off thickness, the effective refractive index is equal to n_s. In this case all the mode power is flowing in the substrate layer, consequently the $\mathrm{Re}(P_c)$ is normally zero. For a relatively very thick guiding layer, the mode power is highly confined in this layer and the $\mathrm{Re}(P_c)$ approaches

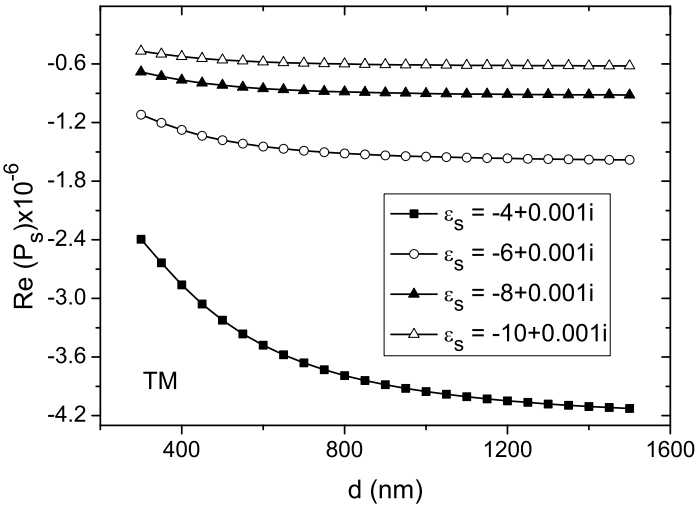

FIG. 11: The real part of the power flowing in the substrate layer versus the thickness of the guiding layer for different values of the substrate permittivity for $\lambda = 632.8$ nm, $n_c = 1.33$, $n_f = 1.75$, and $\mu_s = -1 + 0.001\text{i}$ (TM mode).

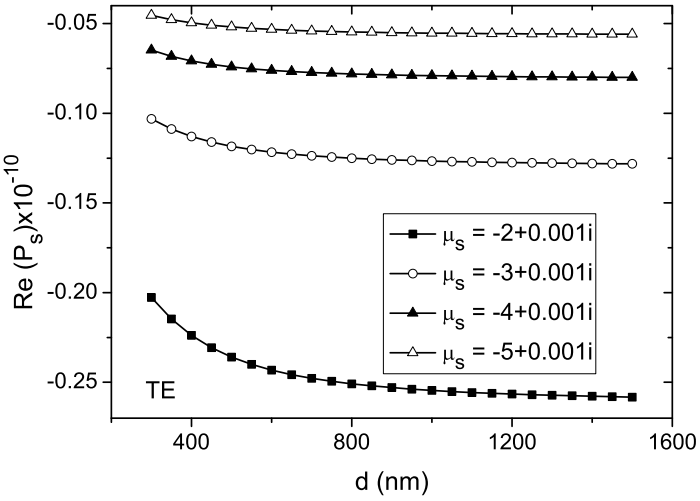

FIG. 12: The real part of the power flowing in the substrate layer versus the thickness of the guiding layer for different values of the substrate permeability for $\lambda = 632.8$ nm, $n_c = 1.33$, $n_f = 1.75$, and $\varepsilon_s = -4 + 0.001\text{i}$ (TE mode).

zero again. Between these two limits, the mode power is distributed among the three layers with a few percent only flowing in the substrate and the cladding.

This behavior undergoes a substantial change when the substrate is made of a LHM.

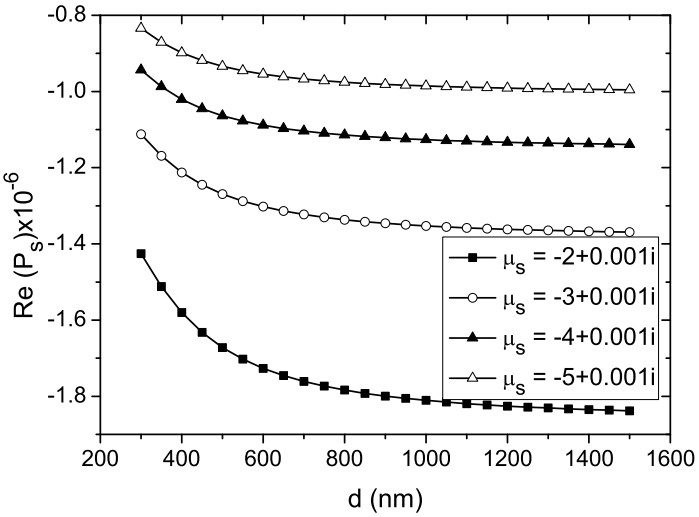

FIG. 13: The real part of the power flowing in the substrate layer versus the thickness of the guiding layer for different values of the substrate permeability for $\lambda = 632.8$ nm, $n_c = 1.33$, $n_f = 1.75$, and $\varepsilon_s = -4 + 0.001$i (TM mode).

As can be seen from the figures (14–17), the Re(P_c) peaks near the cut-off thickness and decays to zero for high thickness. The figures also reveal that the Re(P_c) can be enhanced for some values of ε_s and μ_s to exceed its value in the case of a RHM substrate. This feature is very useful for applications requiring the enhancement of the evanescent field in the cladding.

Therefore, the main difference between the Re(P_c) in RHM- and LHM-substrate structures is at the cut-off thickness. This is simply because in a LHM-substrate structure the effective refractive index of the guided mode can't be under any condition equal to n_s, which is a negative value in this case. Hence, there is no cut-off thickness for the LHM-substrate structure at which the mode is devoted to the substrate. The absence of the cut-off thickness is considered a new feature for the proposed structure.

If we treat the proposed structure as a slab waveguide sensor and plot the sensitivities given by Eqs. (25) and (26) as a function of the guiding layer thickness we obtain Figs. (18–21). The critical dependence of the sensitivity on the fraction of total power flowing in the cladding is obvious. Figures (18–21) show that the sensitivity peaks near the cut-off thickness and decays to zero for high thickness. This behavior of the sensitivity is similar to its behavior in reverse symmetry slab waveguide sensors in which the refractive index of the substrate is taken to be less than that of the cladding [18].

Finally, we plot the penetration depth in the cladding and substrate layers versus the thickness of the guiding layer for different values of ε_s and μ_s, as shown in Figs. 22–25. The penetration depth in the cladding in the case of a RHM substrate begins at low values near the cut-off thickness, peaks at a specific value of the guiding layer thickness, and then decays again at high values of the thickness. This behavior undergoes a substantial change

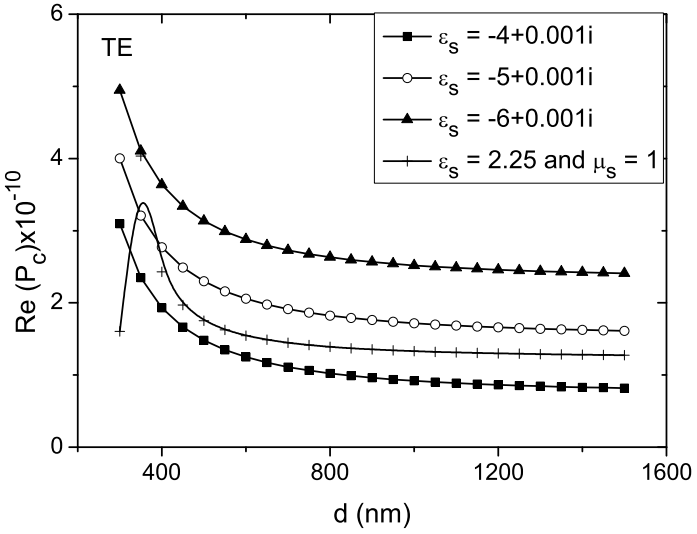

FIG. 14: The real part of the power flowing in the cladding layer versus the thickness of the guiding layer for different values of the substrate permittivity for $\lambda = 632.8$ nm, $n_c = 1.33$, $n_f = 1.75$, and $\mu_s = -1 + 0.001\text{i}$ (TE mode).

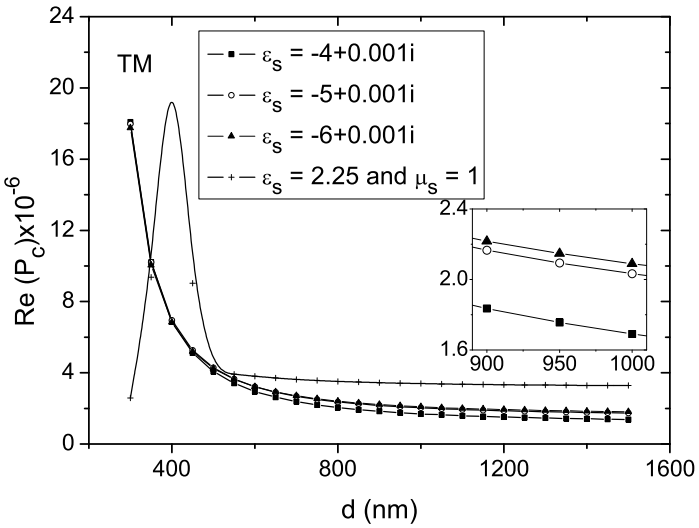

FIG. 15: The real part of the power flowing in the cladding layer versus the thickness of the guiding layer for different values of the substrate permittivity for $\lambda = 632.8$ nm, $n_c = 1.33$, $n_f = 1.75$, and $\mu_s = -1 + 0.001\text{i}$ (TM mode).

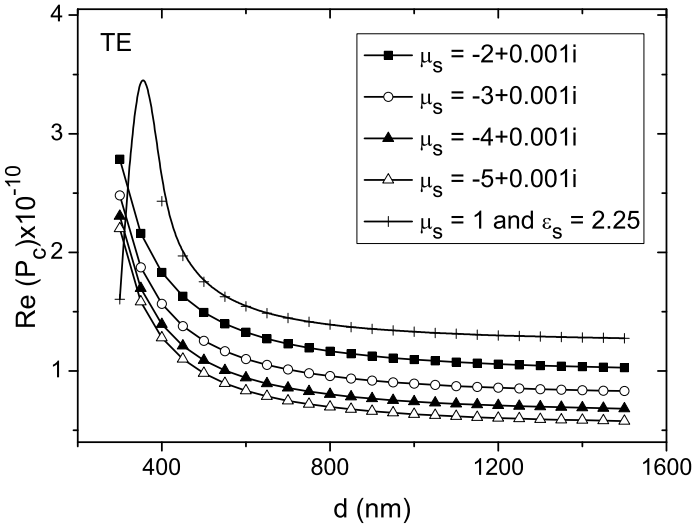

FIG. 16: The real part of the power flowing in the cladding layer versus the thickness of the guiding layer for different values of the substrate permeability for $\lambda = 632.8$ nm, $n_c = 1.33$, $n_f = 1.75$, and $\varepsilon_s = -4 + 0.001\text{i}$ (TE mode).

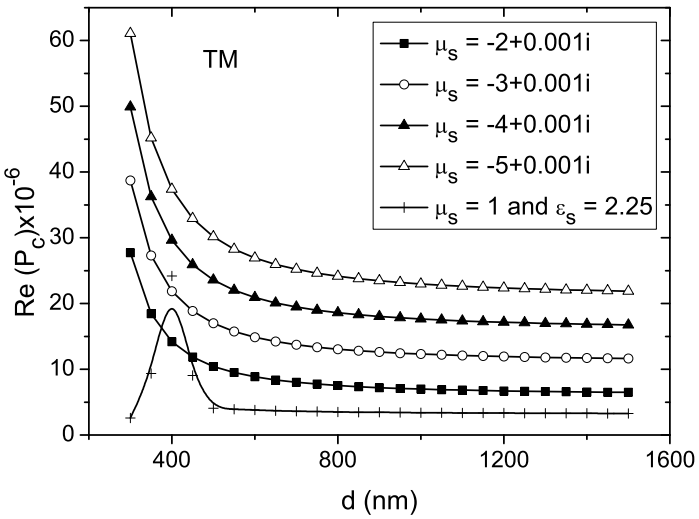

FIG. 17: The real part of the power flowing in the cladding layer versus the thickness of the guiding layer for different values of the substrate permeability for $\lambda = 632.8$ nm, $n_c = 1.33$, $n_f = 1.75$, and $\varepsilon_s = -4 + 0.001\text{i}$ (TM mode).

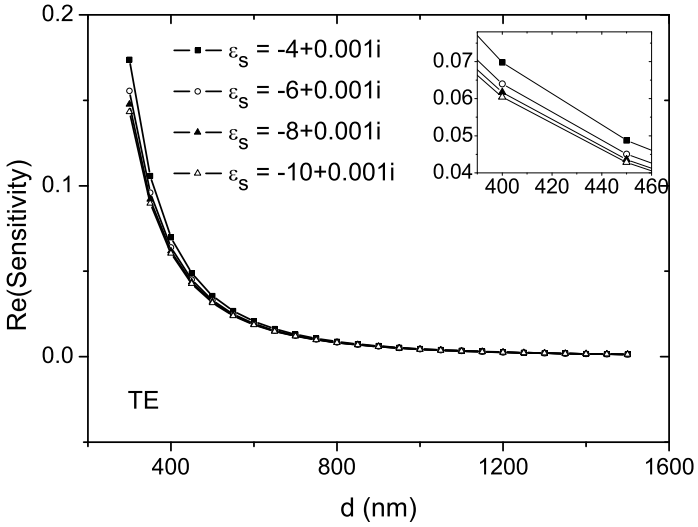

FIG. 18: The real part of the sensitivity versus the thickness of the guiding layer for different values of the substrate permittivity for $\lambda = 632.8$ nm, $n_c = 1.33$, $n_f = 1.75$, and $\mu_s = -1 + 0.001$i (TE mode).

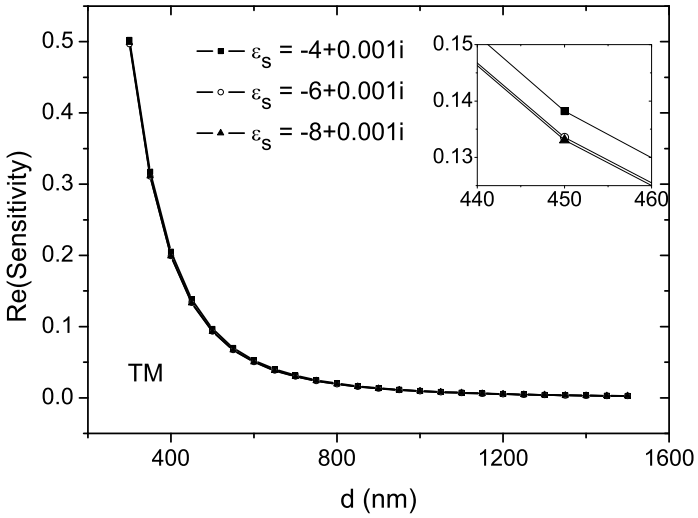

FIG. 19: The real part of the sensitivity versus the thickness of the guiding layer for different values of the substrate permittivity for $\lambda = 632.8$ nm, $n_c = 1.33$, $n_f = 1.75$, and $\mu_s = -1 + 0.001$i (TM mode).

when the substrate is made of a LHM. As can be seen from Figs. 22 and 23, Δx_c peaks near the cut-off thickness and decays for high thickness. Generally, the behavior of Δx_c

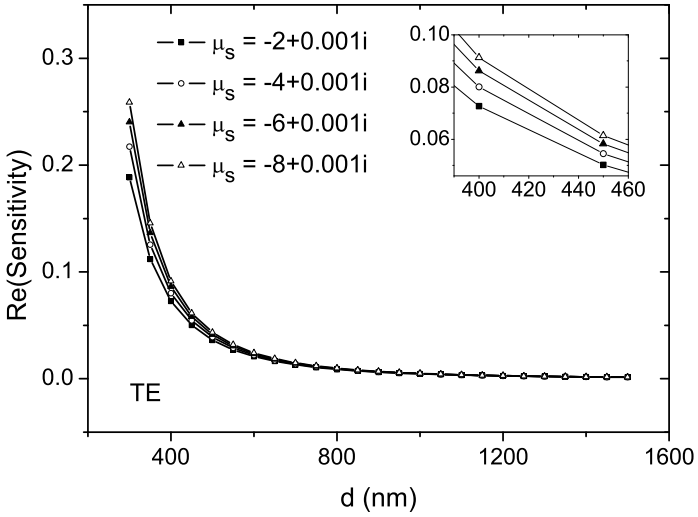

FIG. 20: The real part of the sensitivity versus the thickness of the guiding layer for different values of the substrate permeability for $\lambda = 632.8$ nm, $n_c = 1.33$, $n_f = 1.75$, and $\mu_s = -1 + 0.001$i (TE mode).

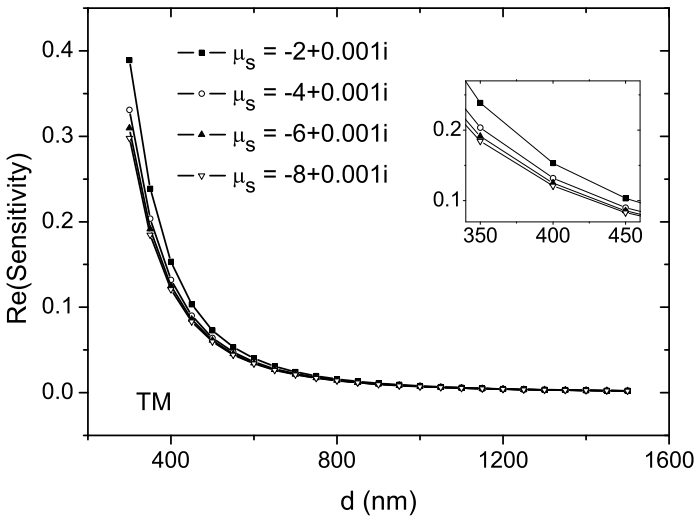

FIG. 21: The real part of the sensitivity versus the thickness of the guiding layer for different values of the substrate permeability for $\lambda = 632.8$ nm, $n_c = 1.33$, $n_f = 1.75$, and $\mu_s = -1 + 0.001$i (TM mode).

is analogous to that of the power flowing in the cladding layer. Similarly, the behavior of Δx_s is analogous to that of the power flowing in the substrate layer, as can be seen from

Figs. 24 and 25.

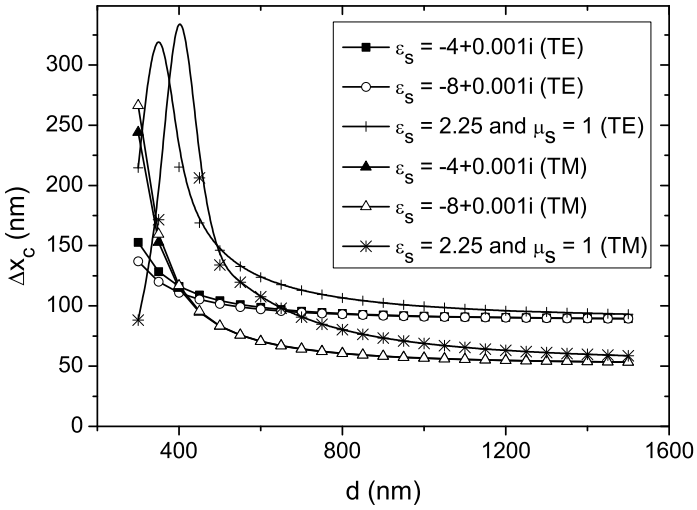

FIG. 22: The penetration depth in the cladding layer versus the thickness of the guiding layer for different values of the substrate permittivity for $\lambda = 632.8$ nm, $n_c = 1.33$, $n_f = 1.75$, and $\mu_s = -1 + 0.001\text{i}$ (TE and TM modes).

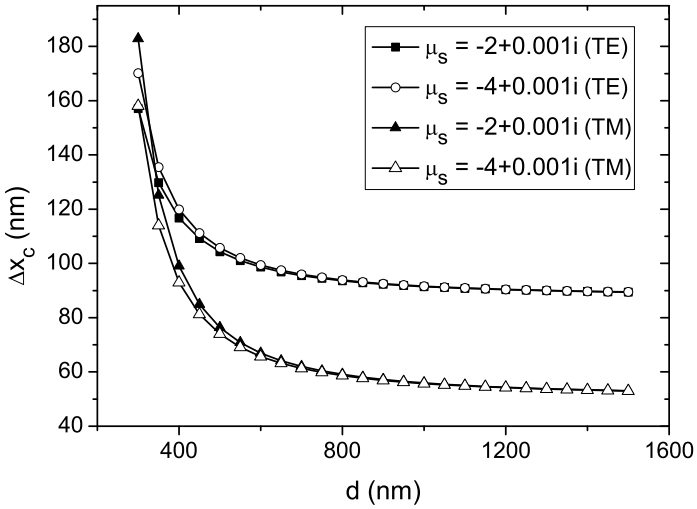

FIG. 23: The penetration depth in the cladding layer versus the thickness of the guiding layer for different values of the substrate permeability for $\lambda = 632.8$ nm, $n_c = 1.33$, $n_f = 1.75$, and $\varepsilon_s = -4 + 0.001\text{i}$ (TE and TM modes).

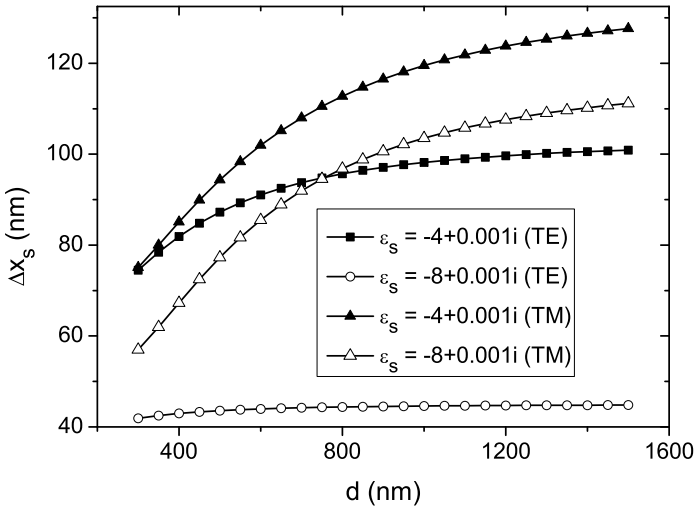

FIG. 24: The penetration depth in the substrate layer versus the thickness of the guiding layer for different values of the substrate permittivity for $\lambda = 632.8$ nm, $n_c = 1.33$, $n_f = 1.75$, and $\mu_s = -1 + 0.001$i (TE mode).

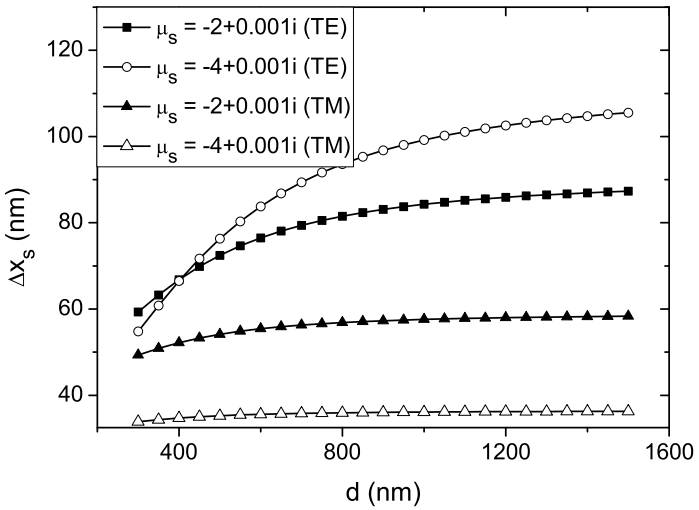

FIG. 25: The penetration depth in the substrate layer versus the thickness of the guiding layer for different values of the substrate permeability for $\lambda = 632.8$ nm, $n_c = 1.33$, $n_f = 1.75$, and $\varepsilon_s = -4 + 0.001$i (TE mode).

IV. CONCLUSION

We have investigated a three-layer slab waveguide structure in which the substrate is made of an isotropic homogeneous lossy LHM. The simulation results have shown many interesting features in the effective index of the structure, power, penetration depth, and sensitivity as a result of the negative parameters of the substrate. The most interesting feature is the enhancement of the power flowing in the guiding layer for specific values of the substrate parameters, which is beneficial for applications requiring high guidance. The power flowing in the cladding layer can also be enhanced for other values of the substrate parameters which is useful for sensing applications.

Finally, it is worth mentioning that we were interested in optical sensing applications in which the cladding usually contains the material to be detected (analyte) which is often a contaminated air or liquid. That is why we have assumed a RHM cladding and a LHM substrate. The analyte can't be a LHM. If we assume a hypothetical structure of LHM cladding and RHM substrate, the above mentioned findings for the evanescent field in the cladding layer are expected to be valid for that in the substrate. This means that the enhancement of the evanescent field in the substrate layer is expected for this hypothetical structure.

References

* Electronic address: staya@iugaza.edu.ps

[1] V. G. Veselago, Sov. Phys. Usp. **10**, 509 (1968).
[2] A. Grbic and G. V. Eleftheriades, J. Appl. Phys. **92**, 5930 (2002).
[3] D. R. Smith and D. Schurig, Phys. Rev. Lett. **90**, 077405 (2003).
[4] I. V. Shadrivov, A. A. Sukhorukov, Y. S. Kivshar, A. A. Zharov, and A. D. Boardman, Phys. Rev. E **69**, 016617 (2004).
[5] V. M. Agranovich, Y. R. Shen, R. H. Baughman, and A. A. Zakhidov, Phys. Rev. B **69**, 165112 (2004).
[6] D. Smith, W. Padilla, D. Vier, S. Nemat-Nasser, and S. Schults, Phys. Rev. Lett. **84**, 4184 (2000).
[7] R. Shelby, D. Smith, and S. Schults, Science **292**, 77 (2001).
[8] O. Voskoboynikov, G. Dyankov, and C. M. J. Wijers, Microelectronics J. **36**, 564 (2005).
[9] J. B. Pendry, Phys. Rev. Lett. **85**, 3966 (2000).
[10] C. Yan, Q. Wang, and Y. Cui, Optik **121**, 63 (2010).
[11] Z. Wang, Z. Zhang, S. Qin, L. Wang, and X. Wang, Materials and Design **29**, 1777 (2008).
[12] Z. Zhang, Z. Wang, and L. Wang, Materials and Design **30**, 3908 (2009).
[13] A. Alu and N. Engheta, Phys. Rev. E **72**, 016623 (2005).
[14] X. M. Zhou and G. K. Hu, Phys. Rev. E **74**, 026607 (2006).
[15] C. Caloz, and T. Itoh, IEEE Microw. Wireless Compon. Lett. **14**, 274 (2004).
[16] S. A. Tretyakov, and M. Ermutlu, IEEE Antennas and Wireless Propagation Letters **4**, 266 (2005).
[17] S. A. Taya, M. M. Shabat, and H. Khalil, Optik **120**, 504 (2009).
[18] S. A. Taya, M. M. Shabat, H. Khalil, and Dieter S. Jäger, Sensor. Actuat. A-Phys. **147**, 137 (2008).

[19] S. A. Taya, M. M. Shabat, and H. Khalil, Optik **121**, 860 (2010).
[20] M. M. Shabat, H. Khalil, S. A. Taya, and M. M. Abadla, Int. J. of Optomechatronics **1**, 284 (2007).
[21] J. Kästel, M. Fleischhauer, S. F. Yelin, and R. L. Walsworth, Phys. Rev. Lett. **99**, 073602 (2007).
[22] V. A. Podolskiy and E. E. Narimanov, Opt. Lett. **30**, 75 (2005).
[23] L. Zhao and T. J. Cui, Appl. Phys. Lett. **89**, 141904 (2006).